The Journal of Chemical Physics

Excess entropy and long-time diffusion in colloidal fluids with short-range interparticle attraction

Cite as: J. Chem. Phys. **150**, 144907 (2019); https://doi.org/10.1063/1.5091564
Submitted: 03 February 2019 . Accepted: 20 March 2019 . Published Online: 11 April 2019

Xiaoguang Ma, Jiachen Liu, Yikang Zhang, Piotr Habdas, and A. G. Yodh

COLLECTIONS

F This paper was selected as Featured

The Journal of Chemical Physics | ARTICLE | scitation.org/journal/jcp

Excess entropy and long-time diffusion in colloidal fluids with short-range interparticle attraction

Cite as: J. Chem. Phys. 150, 144907 (2019); doi: 10.1063/1.5091564
Submitted: 5 February 2019 • Accepted: 20 March 2019 •
Published Online: 11 April 2019

View Online Export Citation CrossMark

Xiaoguang Ma,[1,2,a)] Jiachen Liu,[1] Yikang Zhang,[1,3] Piotr Habdas,[4] and A. G. Yodh[1]

AFFILIATIONS

[1] Department of Physics and Astronomy, University of Pennsylvania, Philadelphia, Pennsylvania 19104, USA
[2] Complex Assemblies of Soft Matter, CNRS-Solvay-UPenn UMI 3254, Bristol, Pennsylvania 19007-3624, USA
[3] Department of Physics, Peking University, Beijing, People's Republic of China
[4] Department of Physics, Saint Joseph's University, Philadelphia, Pennsylvania 19131, USA

[a)] **Electronic mail:** xiaom@seas.upenn.edu

ABSTRACT

Liquid structure and dynamics are experimentally investigated in colloidal suspensions with short-range depletion attraction. The colloidal fluid samples consist of hard-sphere colloidal particles suspended along with rodlike depletants based on surfactant micelles. The spheres have a range of surface chemistries, diameters, and packing fractions, and the rodlike micelle length depends on the temperature. Thus, the combination of hard-spheres and depletants generates a sample wherein short-range interparticle attraction can be temperature-tuned *in situ*. Video optical microscopy and particle tracking techniques are employed to measure particle trajectories from which structural and dynamical quantities are derived, including the particle pair correlation function [$g(r)$], mean square displacement, long-time diffusion coefficient, and the sample two-body excess entropy (S_2). The samples with stronger short-range attractions exhibit more order, as characterized by $g(r)$ and S_2. The stronger short-range attractions are also observed to lead to slower long-time diffusion and more heterogeneous dynamics at intermediate time scales. Finally, the excess entropy scaling law prediction, i.e., the exponential relationship between two-body excess entropy and long-time diffusivity, is observed across the full range of samples.

I. INTRODUCTION

Connecting structure to dynamics is a persistent theme in many studies of condensed matter systems.[1,2] A central idea in this effort is that the interactions between microscopic constituent particles determine material structure, which, in turn, influences material mechanical and dynamical response. One interesting phenomenological theory which seeks to find such connections is based on the concept of excess entropy.[3–6] Excess entropy (S^E) is defined as the difference between the "true" system entropy and the entropy of an equivalent ideal gas system; it is a single number that can be computed from particle position data.[7] The potential value of S^E derives from Rosenfeld's observation,[3] initially supported by simulation data, that transport coefficients of simple liquids such as diffusivity and shear viscosity depend exponentially on S^E. Thus, liquid dynamics are explicitly related to liquid structure via the excess entropy scaling law. This finding provides a simple way to quantitatively estimate long-time dynamical properties in liquids using static structural information.

Following Rosenfeld's initial observation, a physical mechanism for the scaling relation was proposed by Dzugutov. Dzugutov's idea was that diffusivity of liquid atoms should be proportional to the rate of binary collisions and to the number of accessible local configurations. These arguments led to a scaling prediction, $D \sim e^{S^E}$; here, the diffusivity D is normalized by microscopic coefficients[5,8] derived from kinetic theory, and the excess entropy S^E has units of the Boltzmann constant, k_B. Dzugutov's scaling law was subsequently tested in simulations of liquids spanning a variety of interatomic interactions, densities, and temperatures.[5,8] Notably, these studies used the two-body excess entropy, S_2, as an approximation of S^E; S_2 is found to account for more than 90% of S^E in typical liquids and can be computed from a simple integral involving the sample's pair correlation function.[7] The apparent wide applicability of the scaling law resulted in support for the notion that liquid structure determines liquid dynamics, although a more rigorous microscopic justification is desirable. Indeed, mode-coupling theory (MCT), which is well tested in liquids and has proven useful for expressing the self-intermediate relaxation function of constituent particles using their static structure factors,[9] has been applied to obtain excess entropy scaling laws for both the self- and cross-diffusivities. Simulations of pure liquids and binary liquid mixtures with Lennard-Jones (LJ) potentials corroborate MCT predictions[10] and identify the empirical scaling law as a special case. Nevertheless, the structure factors needed for MCT calculations are often highly nontrivial and difficult to evaluate in complex fluids,[9,10] especially for comparison to experiment. Thus, the empirical excess entropy scaling law has remained attractive for its ease of use.

Many successes of the excess entropy scaling are from computer simulations; simulated systems include hard-sphere liquids, liquid metals, Yukawa systems, LJ-like liquids, and liquids with soft-core interactions.[5,11–15] On the experimental side, it has been tested in disordered systems with "repulsive interactions," specifically quasi-two-dimensional (2D) colloidal fluids with short- and long-range repulsion,[16] as well as in 2D granular fluids with hard-sphere repulsion.[17] Less is known about systems with "attractive interactions." Adding attractions to the liquid potential affects both liquid structure and dynamics, and in some cases, the effects due to attraction can be reproduced with an effective repulsive potential.[18–22] "Long-range" attraction effects in the context of excess entropy were studied in a simulated LJ system via comparison to liquid with purely repulsive, inverse 12th-power potentials.[3] This work suggested that the addition of long-range attraction induces "higher" excess entropy and "faster" diffusion, but the scaling form remained the same.

To date, the scaling relation and related phenomenology have not been explored in liquids with "short-range attractions" between constituents. These systems exhibit behaviors that are qualitatively different from liquids with purely repulsive or long-range-attractive constituent interactions. Their investigation is essential for understanding the range of applicability of the excess entropy scaling law. Briefly, short-range attractions strongly affect nearest-neighbor configurations[23] and give rise to interesting structural features in fluids which are precursors of sols and gels.[24–28] Short-range attractions also introduce bonding effects at high packing fractions that give rise to fascinating phenomena such as the re-entrant liquid-glass transition.[29–34]

In this experimental work, we investigate the structure and dynamics in 2D colloidal fluids with tunable short-range attraction, and we critically examine the excess entropy scaling law in this context. From particle trajectory data obtained by video optical microscopy, the particle pair correlation function [$g(r)$], mean-square displacement (MSD), long-time diffusion coefficient (D), and the sample two-body excess entropy (S_2) are determined as a function of packing fraction and interparticle attraction strength. We also calculate a normalized long-time diffusion coefficient, $D^* = D/D_0$, where D_0 is the isolated single particle diffusivity measured at the same temperature and in the same sample cell geometry.

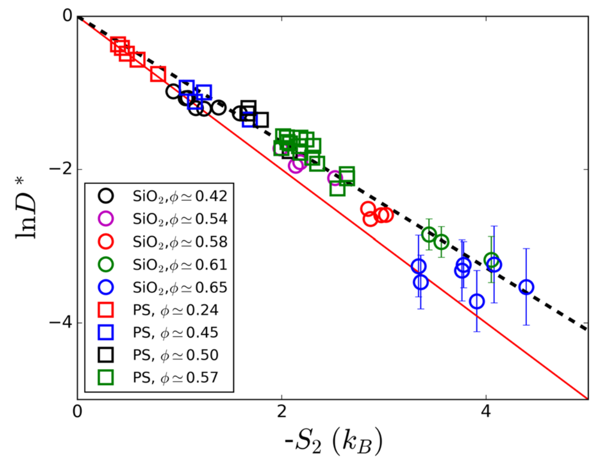

FIG. 1. Normalized diffusion coefficients, $D^* \equiv D/D_0$, as a function of S_2 measured for two types of colloidal particles: SiO_2 (circles) and polystyrene (PS) (squares). For each particle type, colloidal samples of 4–5 different packing fractions are tested; data points from the same sample (i.e., the same packing fraction) are shown by the same color. At each packing fraction, several short-range attraction strengths are studied; data points associated with stronger attractions (but at the same packing fraction) generally show smaller S_2 and D^*. Black dashed line is the best exponential fit, $D^* = e^{0.82 S_2}$. Red solid line indicates $D^* = e^{S_2}$ (see Sec. III D for detailed discussion).

Our central experimental result is shown in Fig. 1. Figure 1 displays D^* vs S_2 from nine samples. These samples are composed of either silica (SiO_2) or polystyrene (PS) particles. Each of the two sample-types (SiO_2 and PS) is studied at many different packing fractions (ϕ) and many interparticle attraction strengths. Across the whole sample set, an exponential scaling law, $D^* \sim e^{cS_2}$, is revealed with $c = 0.82 \pm 0.05$. In addition to this excess entropy result, we observe that stronger short-range attractions induce more ordered and heterogeneous structures within the fluids, as characterized by $g(r)$ and S_2. Moreover, the stronger attractions induce more heterogeneous dynamics at intermediate time scales, as measured by the MSD and non-Gaussian displacement statistics.

The remainder of this paper is organized as follows: We begin with a description of sample preparation, sample characteristics, and experimental methods. Then, we characterize the colloidal fluid structure using $g(r)$ and S_2, and we identify trends associated with increasing short-range attraction strength and packing fraction. The diffusion dynamics of isolated particles and particles in concentrated suspension are described next, including diffusion coefficients in the long-time limit and heterogeneous dynamics at intermediate time scales. The results provide insights about the attractive fluids and are finally utilized to directly test the scaling law under a wide range of experimental conditions with varying excess entropy. Finally, we summarize the results and discuss future work.

II. EXPERIMENT

We introduce and control the short-range attractions between colloidal particles utilizing micelles composed of hexaethylene

TABLE I. Colloidal particles used in the experiment.

Sample	Spacing (μm)	Particle	σ (μm)	NaCl (mM)
SiO_2	150-160	SiO_2	2.0	2.0
PS	1.1-1.4	PS-COOH	1.0	0.0

glycol monododecyl ether ($C_{12}E_6$) surfactant molecules.[35–37] The concentration of $C_{12}E_6$ in the aqueous solution is 44 mM, much larger than the critical micelle concentration[38] (CMC) of 0.072 mM at 25 °C. At such high concentrations, the $C_{12}E_6$ molecules self-assemble into rodlike micelles.[37] The depletion force induced by the micelles is temperature-tunable because the micelle length increases with solution temperature. A small amount (2 mM) of sodium chloride (NaCl) is added to the sample solutions which gives rise to a Debye screening length, κ^{-1}, of 7 nm.[39] This Debye screening length increases the "effective" dimensions of the micelle rods beyond their bare values, which in turn affects the strength and range of the depletion force induced by the micelles.[37] Thus, salt concentration can also be utilized to fine-tune the short-range attraction between colloidal spheres. Experimentally, we find that higher salt concentrations give rise to stronger short-range attractions. In this experiment, however, high salt concentrations are avoided because they also promote particles sticking to the glass cover slips. Two types of colloidal spheres (plain silica and carboxylated polystyrene) are used in the experiment. Their physical properties are listed in Table I.

The plain silica (SiO_2) spheres have a nominal diameter σ = 2.0 μm (Corpuscular, Inc.). For sample preparation, we dissolve this SiO_2 particle solution in deionized (DI) water and remove the residual impurities by repeated centrifugation (10 times). The cleaned particle solution is then filled in a 15 ml centrifuge tube for free sedimentation, which continues until the interface between the supernatant and particle-containing solution fall to around 1/2 of its original height. Finally, 100 μl of the solution just below the interface is collected using a pipette. As a result of this procedure, a very monodisperse distribution of single particles remains.

The SiO_2 sample solution is then introduced into a homemade sample cell shown in Fig. 2(a). The cell chamber is formed by the parallel surfaces of two glass cover slips (No. 1.5, Thermo Fisher) that are separated by 160 μm-thick spacers. The cell chamber is filled with a small amount of SiO_2 sample solution from the front opening and then sealed peripherally using UV-cured optical glue (Norland 65). The gravitational length, $L_g \equiv k_B T/(\Delta\rho V g)$, is estimated to be 0.1 μm for the SiO_2 particles; here, k_B is the Boltzmann constant, T is the temperature, $\Delta\rho$ is the difference between the densities of silica and water, V is the hard-sphere volume of the particle, and g is the gravitational constant. The small L_g implies that the SiO_2 particles will readily sediment and form a monolayer near the glass surface at the bottom of the cell. The packing fraction, ϕ, of the colloidal monolayer is controlled by using sample solutions with different particle concentrations.

The carboxylated polystyrene (PS) latex beads have a nominal diameter, σ = 1.0 μm (Thermal Scientific). Procedures very similar to those used for the SiO_2 particles (see above) are employed to clean the PS particle solution and filter out particle aggregates. Since L_g for the PS particles is approximately 20 μm, the particles will not form a monolayer due to gravity alone. Therefore, a different type of sample cell is needed for PS particles, which is shown schematically in Fig. 2(b). We sandwich a droplet (0.5–0.7 μL) of PS particle solution between two glass cover slips. The two cover slips bind together via capillary forces. The cell is then sealed on its periphery using optical glue. For the detailed experimental studies, we select regions in the cell wherein all particles are in focus and wherein positional fluctuations along the vertical axis are not apparent. The separation between glass surfaces, within this field of view, is estimated manually by focusing on dust on both surfaces and scanning from one surface to the other. This method gives a rough estimate for chamber thickness in the range of 1.1–1.2 μm.

The sample cells are then placed on the stage of an inverted microscope (Zeiss Axiovert 135). Brownian motion is observed through a 100× oil-immersion objective (NA = 1.3). The sample temperature is maintained and adjusted between 20 and 34 °C by an objective heater (PeCon GmbH) with 0.1 °C resolution. Movies of particle motion within the field of view are recorded under bright-field illumination at a resolution of 2592 × 1944 pixels and at a rate of 10 frames/s using a monochrome CMOS camera (SV5M10, SILICON VIDEO). The recording time for each experiment ranged between 10 and 30 min, depending on the sample 2D packing fraction.

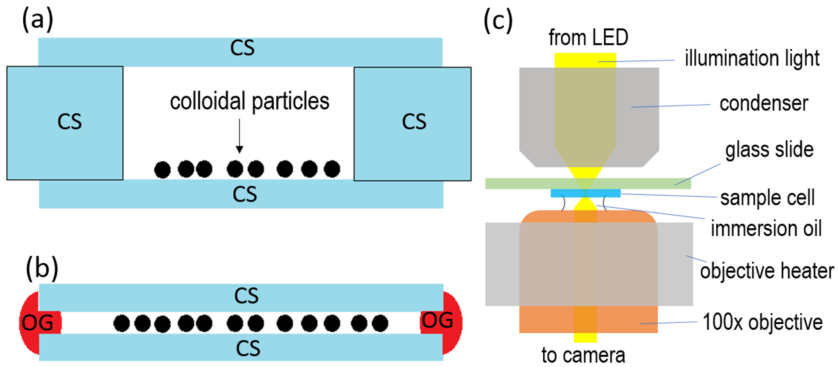

FIG. 2. Schematics of the cells used for (a) SiO_2 particle-containing samples and (b) PS particle-containing samples (CS: glass cover slip, OG: optical glue). (c) Schematic of the sample cell in the microscope stage.

III. RESULTS AND DISCUSSION

A. Temperature-dependent pair potentials

The new feature of this work compared to other excess entropy experimental studies is the short-range attractive potential between particles. We discuss this potential in detail in this subsection. The geometric properties of the rodlike $C_{12}E_6$ micelles are described briefly below and are described in detail in prior publications.[36–38] At temperatures > 20 °C, the micelles evolve from spheres into cylinders with hemispherical caps at two ends. The cross-sectional diameter of the cylinder is d_{cs} = 4.3 nm and is independent of temperature, but the average length, L, of the micelle rods grows with increasing solution temperature. For example, at 44 mM concentration of $C_{12}E_6$, L increases from 19 nm at 22 °C to 31 nm at 28 °C.[37] The changing aspect ratio, L/d_{cs}, of the micelle rods provides a way to vary the depletion force between colloidal particles. Two models are usually employed for calculating the pair-potential between colloidal particles in the presence of rodlike depletants. For small aspect ratios ($L/d_{cs} \simeq 1$), the depletants are best modeled as ellipsoids,[40] while for larger aspect ratios ($L/d_{cs} \gg 1$), a thin-rod model becomes more accurate.[41] It was shown previously[37] that the ellipsoid model describes the measured pair-potentials between silica spheres suspended in $C_{12}E_6$ solutions for L/d_{cs} between 4.4 and 7.2. In this study, we employ this well-understood attraction effect empirically, and we characterize the pair-potential, $U(r)$, by direct measurements.

We measure the particle pair correlation function, $g(r)$, in dilute samples. For this measurement, the packing fraction, ϕ, of the colloidal monolayer is kept below 0.01 to minimize effects due to many-body interactions. (Note, distortions in the measured $g(r)$ due to optical artifacts are corrected following Ref. 42.) Figure 3(a) shows the corrected $g(r)$ from the PS samples at different temperatures ranging from 21 °C to 31 °C. Notice, the first peaks of $g(r)$ grow with increasing temperature; thus, the probability of finding particle pairs temporarily bonded together is enhanced at higher temperatures. The first peak location (in units of normalized particle-particle separation, r/σ) varies between 1.08 and 1.1. It shifts to slightly shorter separations when the temperature is increased. This behavior is driven by a force balance at a short-range between the repulsive screened Coulomb force and the attractive depletion force. The carboxyl group (-COOH) on the surfaces of PS particles is negatively charged in our aqueous solutions, and the range of the screened Coulomb repulsion is approximately $r/\sigma \simeq 1.1$, corresponding to the position of the first peak of $g(r)$ at 21 °C, when the depletion attraction is negligible. When the attraction is increased at higher temperatures, the force balance shifts the equilibrium particle-particle separations to shorter distances. These observations are consistent with previous measurements.[37]

The pair-potential, $U(r)$, is computed from $g(r)$ via the Boltzmann distribution, i.e., $U(r) = -k_BT \ln[g(r)]$. The results are shown in Fig. 3(b). The depth of $U(r)$, i.e., $U_{\min}$, becomes larger with rising temperature; thus, the attractive force between colloidal particles becomes stronger at higher temperatures. Moreover, the width of the potential well becomes wider at higher temperatures, indicating that the depletion interaction range is larger with longer rodlike micelles. The extracted $U_{\min}$ from $U(r)$ measured at different temperatures, is shown in Fig. 3(c). Within the experimental range, $U_{\min}$ is a linear function of temperature, growing from 0 to 4.8 k_BT. The linear relation between attraction strength and temperature in polystyrene spheres is similar to previous silica-sphere experiments,[37] although the absolute magnitudes are different due to different colloidal particle sizes, surface charges, and screening lengths.

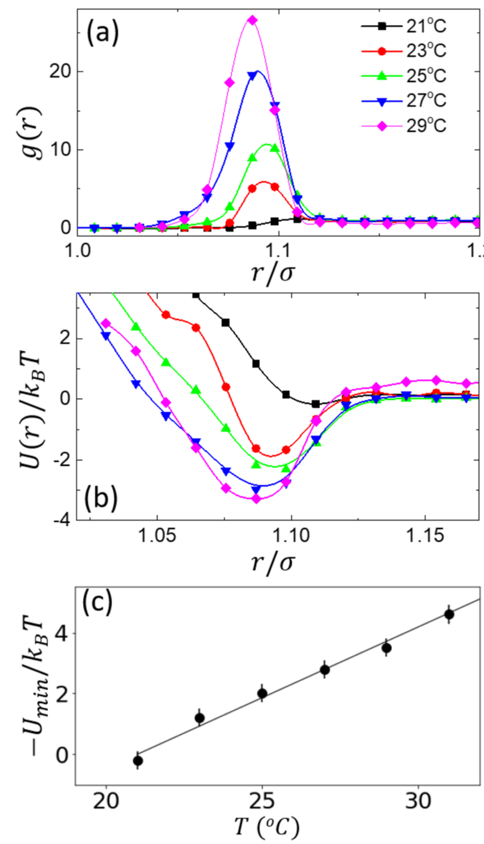

FIG. 3. (a) Measured pair correlation function, $g(r)$, at different temperatures. (b) Interparticle potential, $U(r)/k_BT = -\ln[g(r)]$ vs r/σ, at different temperatures. (c) The attraction strength, $U_{\min}$, defined as the minimum value of $U(r)$ at different temperatures. The solid line is a linear fit.

The $U(r)$ measured from dilute samples characterizes the temperature-dependent depletion-induced attraction. Note, in dense colloidal suspensions, it is more difficult to extract $U(r)$ from $g(r)$ because the latter is strongly influenced by many-body interactions. Nevertheless, for our discussions, we will assume that the temperature-dependent trend of the depletion force at dilute concentration remains qualitatively the same at all packing fractions. Therefore, in the following, we use temperature, T, to represent the relative strength of depletion force for samples with the same packing fraction and particle type.

B. Pair correlation functions and excess entropy

At the packing fractions used in most of the experiments, the structure in the colloidal suspensions is determined by both interparticle depletion attraction and excluded-volume effects typically associated with hard spheres. In this section, we examine the influence of attractive forces relative to excluded-volume effects on colloidal fluid structures. We utilize a subset of the whole dataset here to demonstrate trends while keeping the presentation simple and clear. Specifically, we obtain data [i.e., $g(r)$] which exhibit systematic variation as a function of sample temperature at a constant packing fraction; we also compare these variations for samples at two different packing fractions. This subset of data exhibits the major trends of our full set of samples, which span the full range of temperatures and packing fractions (up to $\phi \simeq 0.65$) for both particle types.

Figure 4 shows the measured $g(r)$ of a subset of PS samples in the temperature range from 22 °C to 28 °C. For clarity, only four temperatures are shown. Two packing fractions, $\phi \simeq 0.24$ and $\phi \simeq 0.57$, are selected to compare the effects of attraction on $g(r)$ in semidilute vs concentrated colloidal fluids. For each packing fraction, the experimental data are collected from exactly the same region within the sample.

Figure 4(a) shows $g(r)$ for the lower packing, $\phi \simeq 0.24$. When attraction strength is increased, $g(r)$ exhibits notable changes. The height of the first peak of $g(r)$ increases from 2 at 22 °C to 4 at 28 °C. This increase implies that, on average, particles have more neighbors in close proximity with stronger attraction, as is qualitatively apparent in the images shown in the insets of Fig. 4(a). Note, one should not confuse this stronger local order with a similar effect induced by increased packing fractions; the former is caused by the extended lifetime of the transient "bonds" due to the short-range attractions, while the latter is caused by an increase in the overall particle density. Besides the first peak, we also observe a slight decrease in $g(r)$ for particle separations just beyond the immediate neighborhood [between $r = 1.2\sigma$ and $r = 1.7\sigma$, see Fig. 4(a)]. This phenomenon can be rationalized from particle density conservation. The fixed packing fraction requires that an enhanced particle density at the nearest-neighbor distance [i.e., reflected in the first peak of $g(r)$] should be compensated by decreased densities elsewhere. Stronger attractions prevent nearest-neighbor particles from diffusing away and leave the space beyond the nearest-neighbor distance more empty. We do not observe any measurable change in $g(r)$ beyond the second peak, consistent with the short-range nature of the interparticle attraction. At much higher temperatures (e.g., >32 °C), we observe particle aggregates that persist longer than the experiment duration (10 min). The $g(r)$ measured from these suspensions with aggregated particles preferentially samples dense nonequilibrium local environments. Thus, experimental suspensions containing these quasi-permanent aggregates (at the highest temperatures) are excluded from our analysis of structure and dynamics.

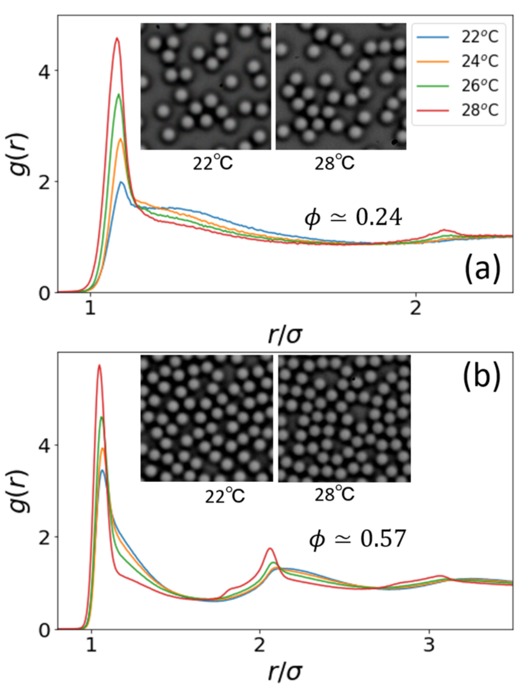

FIG. 4. (a) Measured pair correlation function, $g(r)$, from PS samples at packing fraction $\phi \simeq 0.24$ for different temperatures. Insets show microscopic images of the sample at 22 °C and 28 °C, respectively. (b) Measured $g(r)$ from PS samples at packing fraction $\phi \simeq 0.57$ for different temperatures. Insets show microscopic images of the sample at 22 and 28 °C, respectively.

Figure 4(b) shows a similar $g(r)$ dataset, this time measured at $\phi \simeq 0.57$ from PS samples. The temperatures are the same as in Fig. 4(a), and the temperature-dependent attraction strength is assumed to be the same as in Fig. 4(a). Since the colloidal samples are more concentrated, long-range order emerges in the measured $g(r)$ [Fig. 4(b)]. As in Fig. 4(a), the first peak of $g(r)$ grows, from 3.5 at 22 °C to 6 at 28 °C. The width of the first $g(r)$ peak also becomes narrower with increasing temperature, indicating stronger local ordering. In addition, the second and third peaks are observed to grow with increasing temperature and shift to shorter separations; this effect diminishes at longer distances. These changes in $g(r)$ are indicative of the formation of transient particle clusters at stronger attraction. This aggregation is apparent in the images of the insets of Fig. 4(b), which show particle configurations at both 22 °C and 28 °C. Specifically, they show that particles form more ordered clusters with three-fold symmetry at a higher temperature, and for the same temperature, the cluster sizes are larger than those formed at lower packing fractions [see insets in Fig. 4(a)]. For more concentrated packing fractions ($\phi > 0.65$) or much higher temperatures ($T > 32$ °C), we observe large domains of colloidal crystals with lifetimes longer than the experiment duration (up to 30 min). Again, data from samples containing these quasi-permanent domains are excluded from the remaining analyses.

The pair correlation functions suggest that the structure of the colloidal fluid is largely determined by sample packing fractions. The short-range attractions modify $g(r)$ to a lesser degree and in different ways. Specifically, the depletant-induced attractions enhance all peaks in $g(r)$ and shift peak positions to shorter distances. These trends are present in samples with different packing fractions, different particle types (SiO_2 and PS), and different sample cell geometries.

The two-body excess entropy (per-particle), S_2, is readily computed from the measured $g(r)$ using the integral[58]

$$S_2 = -\pi N \int_0^\infty \{g(r)\ln[g(r)] - [g(r) - 1]\} r dr. \quad (1)$$

Here, N is the number density of particles in the colloidal fluid. This relationship characterizes and permits comparison of S_2 values among colloidal fluids with different packing fractions and attraction strengths. Figure 5(a) shows the computed S_2 in the fluid of PS spheres with packing fraction $\phi \simeq 0.24$ (for the same temperatures as in Fig. 4). S_2 is negative because the reference ideal gas entropy has the maximal value. A smaller (more negative) value of S_2 is thus indicative of a more ordered sample. Figure 5(a) shows that S_2 decreases with increasing temperature, reflecting the fact that colloidal fluids with the same particle density become more ordered with increased interparticle attraction. Notably, this finding is in stark contrast to the effect of added long-range attractions. Added long-range attractions "increase" S_2; typically, these long-range attractions are well described by mean field theory[18,19] and effectively reduce the influence of short-range repulsion.[3] By contrast, short-range attractions are always localized and are not well described by an approximate (adjusted) mean-field repulsion. Figure 5(b) shows S_2 computed for a PS sample at higher packing fraction $\phi \simeq 0.57$. Similar trends between S_2 and temperature are observed. Note, however, at a higher packing fraction, the absolute value of S_2 is larger than the corresponding data in Fig. 5(a) at each temperature. This observation suggests that the packing fraction is the primary factor that affects entropy in the colloidal fluids and is consistent with the conjecture that $g(r)$ is mostly determined by sample packing fraction (see Fig. 3).

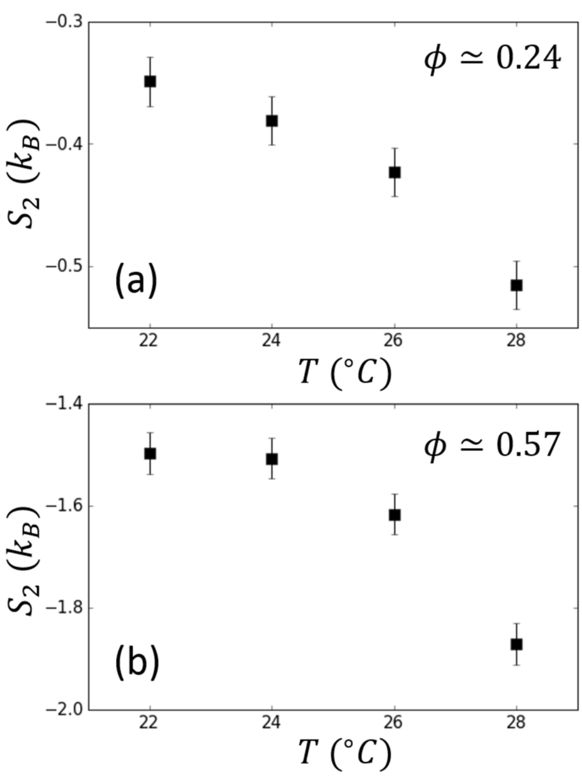

FIG. 5. (a) The two-body excess entropy, S_2, measured for PS samples at lower packing fraction $\phi \simeq 0.24$ and at different temperatures. (b) S_2 measured for PS samples at higher packing fraction $\phi \simeq 0.57$ and at different temperatures.

C. Diffusion dynamics

To compare transport coefficients among various systems, different normalization factors (D_0) have been proposed to correct the absolute diffusion coefficients and shear viscosities.[4,5] Interestingly, the discussion in Ref. 4 suggests that the choice of D_0 determines the prefactor c in the scaling form: $D/D_0 \simeq e^{cS_2}$. In our experiment, we choose D_0 to be the single-particle diffusion coefficient measured at dilute particle concentration. D_0 is associated with the natural time scale due to Brownian motion and has been widely used as a normalization factor for diffusivities in colloidal suspensions.[16,43–47] Another benefit of using D_0 is that the scaling law is automatically satisfied in the dilute gas state where $S^E \simeq 0$ [i.e., $D(\phi \simeq 0)/D_0 \simeq e^0$].

Therefore, the first step in our analysis of sample dynamics requires measurement of D_0 at dilute concentration as a function of temperature. These D_0 values account for potential hydrodynamic drag effects in each cell. The long-time diffusion coefficients, D, measured at higher concentrations are normalized by D_0 to give $D^* = D/D_0$. D^* is then utilized in the excess entropy scaling relationship. For colloidal particles without attractive forces, this measurement of D_0 is easily done using very dilute suspensions ($\phi < 0.005$). When attractions are present, particles can form transient clusters (see Figs. 3 and 4), and the particles within these clusters diffuse slower than single (free) particles. Therefore, to most accurately measure D_0, we first identify all pairs of particles that have separations smaller than 1.5σ, and we remove these particles (in clusters) from our trajectory data. This procedure ensures that the remaining particle trajectories contain only the dynamics of single (free) particles.

To illustrate the small cluster effect, we compare the MSD dynamics with and without cluster contributions. The MSDs for two groups are shown in Fig. 6(a) for PS samples with $\phi \simeq 0.003$, at 22 °C and 30 °C. At 22 °C, the MSDs derived from data with and without cluster subtraction are very similar because the attractions are weak and the number of clusters are very small. At 30 °C (strong attraction), however, the MSD curves are clearly different with and without cluster subtraction. Diffusion coefficients are calculated from the MSDs using the relation $D_0 = \langle \Delta r^2(t) \rangle/(4t)$. The resulting diffusion coefficients, with and without clusters, are shown in Fig. 6(b) for all temperatures. Notice, the diffusivity measured from samples of single (free) particles is always larger than or equal (within error bars) to the diffusivity derived from the same samples with clusters included. These differences become larger at higher temperatures wherein the attraction strength is stronger. The single (free) particle diffusion coefficient exhibits a very weak dependence on temperature [red circles in Fig. 6(b)]. This slight observed decrease in diffusivity at higher temperatures might be due to the shorter separations between the particles and the glass substrate that arise when attractions become stronger.[48] Other factors also affect single particle diffusion. For example, water viscosity decreases by 15% across this temperature range (from 22 °C to 30 °C), a phenomenon which would partially compensate the effects of particle-wall separation variation. Regardless, since long-time diffusion coefficients are normalized by the single (free) particle diffusion coefficient at the same temperature and within the same sample cell, the effects of solvent viscosity and particle-substrate hydrodynamics are expected to scale out.

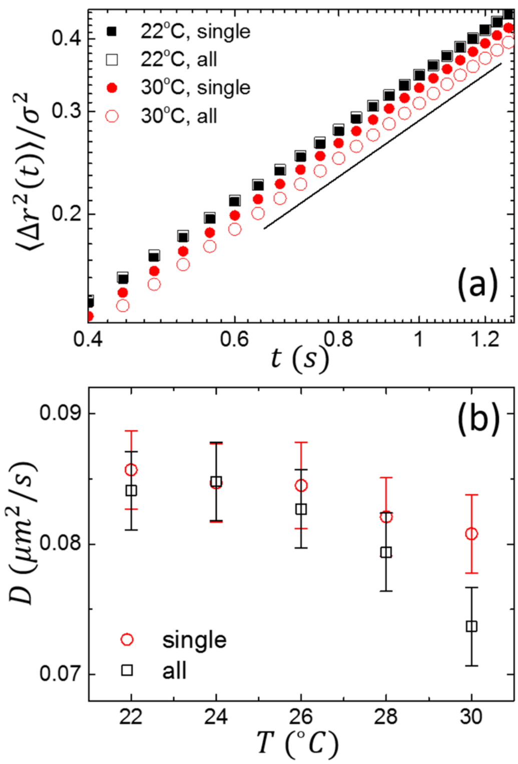

FIG. 6. (a) Measured MSDs from PS samples with packing fraction, $\phi \simeq 0.003$, at two temperatures. The MSD are in units normalized by the particle diameter squared, σ^2. Filled symbols denote data obtained with only single particles included in the analysis, and open symbols denote data obtained with all particles (single and clustered) included in the analysis. The black solid line has unity slope on the log-log scale. (b) Diffusion coefficients derived from the MSDs of each sample as a function of temperature. The difference in diffusion coefficients for data based on all particles (black squares) and single particles only (red circles) is shown.

In the concentrated colloidal fluids, the particles diffuse much slower because of "crowding" effects. In addition, transient clusters form due to short-range attractions and provide a second, qualitatively different, mechanism to slow particle dynamics. Here, we evaluate the influence of attraction strength on particle dynamics in the semi-dilute and dense colloidal fluids. Figure 7 shows MSDs measured from PS samples with packing fraction $\phi \simeq 0.24$ at temperatures ranging from 22 °C to 30 °C. The slopes of the MSD curves decrease with stronger attraction. Thus, particle dynamics are more hindered by the stronger attractive forces. The MSD curves are well fit by straight lines, suggesting their dynamics are diffusive. The long-time diffusion coefficient, D, is calculated from data with $t > 100$ s using the relation $D = \langle \Delta r^2(t) \rangle/(4t)$. These long-time diffusion coefficients decay monotonically with increasing temperature, as is shown in the inset of Fig. 7. Again, we note that the effect of adding short-range attractions is "opposite" to that of adding long-range attractions which increase diffusion coefficients.[3]

Figure 8 shows MSDs measured from PS samples with packing fraction $\phi \simeq 0.57$. These MSD curves exhibit subdiffusive behavior at short lag times ($t < 150$ s). At longer lag times ($t > 200$ s), the slopes of the MSD curves become unity on the log-log scale. Thus, particle motions are diffusive in the long-time limit. We fit the long-time ($t > 200$ s) MSD data to obtain the long-time diffusion coefficients shown in the inset of Fig. 8. The measured D decreases as the temperature is increased, again confirming that particle long-time diffusion dynamics become slower with stronger short-range attractions. At corresponding temperatures, the particle diffusion coefficients at $\phi \simeq 0.57$ are smaller than those at $\phi \simeq 0.24$ due to "crowding" effects, as expected. We exclude more concentrated samples ($\phi > 0.65$) from our analysis. In these dense samples, we are not able to measure long-time diffusion coefficients because particles in the crystal domains do not diffuse significantly within the experiment time. Note also, at much higher packing fractions ($\phi > 0.75$), anomalous re-entrant dynamics have been observed in 2D monodisperse ellipsoidal fluids.[33] Our experiments are carried out in the low packing regime ($\phi \leq 0.65$), where

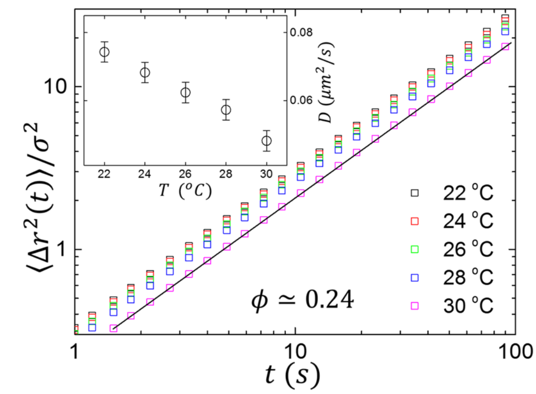

FIG. 7. Measured MSDs from PS samples at packing fraction $\phi \simeq 0.24$ for different temperatures. The MSDs are expressed in units normalized by the particle diameter squared, σ^2. The black solid line has unity slope on the log-log scale. Inset shows the measured D as a function of temperature (T).

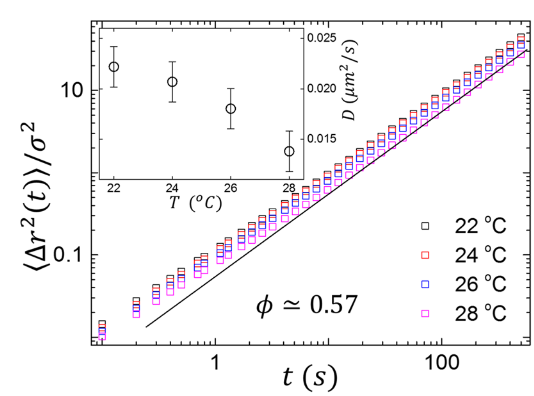

FIG. 8. Measured MSDs from PS samples at packing fraction $\phi \simeq 0.57$ as a function of temperature, T. The MSDs are expressed in units normalized by the particle diameter squared, σ^2. The black solid line has unity slope on the log-log scale. Inset shows the measured long-time D ($t > 200$ s) as a function of T.

anomalous dynamics are not found. Future studies to compare dynamics of 2D spherical particle fluids with 2D ellipsoidal and 3D spherical particle fluids in the dense anomalous regime[30,31,33] should be interesting.

The clusters that form with stronger attractive forces (see, e.g., Figs. 3 and 4) are indicative of heterogeneous structures within the colloidal fluids. Indeed, these clusters may be indicative of heterogeneous dynamics too. To quantify the heterogeneity in dynamics, we compute the non-Gaussian parameter, $\alpha_2(t) \equiv 2\frac{\langle \Delta r^4(t)\rangle}{\langle \Delta r^2(t)\rangle^2} - 4$, which is readily derived from particle trajectories. α_2 quantifies the deviation of the probability density function (PDF) of particle displacements from Gaussian statistics. In supercooled colloidal fluids, a large α_2 value was found to be associated with the heterogeneous particle dynamics.[49,50] Figure 9(a) shows the measured $\alpha_2(t)$ from PS samples with $\phi \simeq 0.24$. The α_2 are significant, indicating heterogeneous dynamics; they first increase and then decrease over the full experimental time scale for samples at all temperatures. The peak in the measured α_2 indicates the lag time at which the dynamics become most heterogeneous. These time scales, which correspond to the α_2 peaks, appear to shift slightly from 1.5 s at 22 °C to 0.7 s at 28 °C. Moreover, the α_2 are larger at higher temperatures, suggesting that more heterogeneous dynamics are also associated with stronger attractions and more heterogeneous structures.

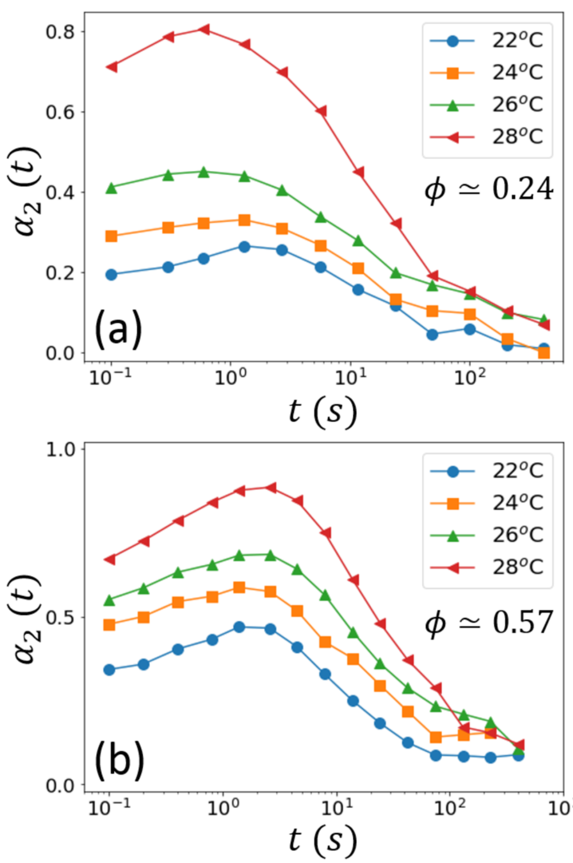

FIG. 9. (a) Measured non-Gaussian parameter, $\alpha_2(t)$, vs lag time from PS samples at packing fraction $\phi \simeq 0.24$. (b) Measured $\alpha_2(t)$ vs lag time from PS samples at packing fraction $\phi \simeq 0.57$.

Figure 9(b) shows the measured $\alpha_2(t)$ from PS samples with $\phi \simeq 0.57$. In this case, α_2 exhibits peaks around 3 s, which is longer than the peak times in Fig. 9(a). Furthermore, the α_2 are greater when the sample temperature is higher, confirming that stronger attractions induce more heterogeneous dynamics at both colloid concentrations. At much longer times ($t > 200$ s), the α_2 curves decay to below 0.1, indicating that particle dynamics are becoming homogeneous again. Notice also, the MSDs start to exhibit unity slope (see Fig. 8) only after the dynamics becomes homogeneous (e.g., $\alpha_2(t) < 0.1$).

D. Scaling of diffusion and excess entropy

Finally, we use the detailed data about single particle dynamics and fluid structure to test the excess entropy scaling relation, which we foreshadowed in the introduction. To this end, the normalized long-time diffusion coefficients, $D^* \equiv D/D_0$, are determined for SiO_2 and PS samples, with packing fractions ranging from $\phi \simeq 0.24$ to $\phi \simeq 0.65$ and with temperatures (attraction strength) ranging from 22 °C to 32 °C. The computed D is plotted as a function of S_2 in Fig. 1. Note, five different packing fractions were studied for the SiO_2 samples (circles in Fig. 1) and four different packing fractions were studied for the PS samples (squares in Fig. 1). Data points from the same sample (i.e., same particle type and same ϕ) but at different temperatures are labeled with the same color; these data points spread out in the plot because the temperature-dependent short-range attractions affect both D^* and S_2.

The data collapse onto a master curve whose best exponential fit, $D^* = e^{cS_2}$ ($c = 0.82 \pm 0.05$), is shown as the black dashed line in Fig. 1. For comparison, Dzugutov's scaling law ($c = 1.0$) is also plotted in Fig. 1 (red solid line). The computed chi-square goodness of fit, $\chi^2 = \sum_{S_2} \frac{(\ln D^* - cS_2)^2}{|cS_2|}$, are 0.9 and 3.4 for the two scaling forms with $c = 0.82$ and $c = 1.0$, respectively. Clearly, the data deviate from Dzugutov's original scaling law ($c = 1.0$). As shown in Figs. 4 and 5, data from the same sample exhibit smaller D^* and smaller S_2 when attraction is stronger (higher temperature). The data points from various temperatures follow the scaling law accurately, especially for $S_2 > -3$. Note, data at much smaller S_2 are derived from samples with very high packing fractions ($\phi > 0.6$); in these cases, the measured standard error for the long-time diffusion coefficients becomes significantly larger because the diffusion in this regime is very slow.

Our results support the notion[3,5] that, even in fluids with substantial short-range interparticle attraction, the particle diffusion coefficients increase monotonically with the number of local accessible configurations (Σ), i.e., $\Sigma = e^{S^E}$. We do not fully understand the origin of the exponential prefactor c. As mentioned earlier, the choice of the normalization factor (D_0) can affect the value of c.[4] In addition, many-body hydrodynamic interactions in confined spaces also affect diffusion, but a consensus about the effect of hydrodynamic interactions on the long-time diffusion remains to be established.[44–46,51] When D_0 is chosen to be the single particle diffusivity, previous experiments have demonstrated that c is sensitive to the hydrodynamic boundary conditions associated with various interfaces.[16] The c value obtained here is in the same range as reported previously in a similar sample cell geometry but without interparticle attraction. When $c = 1$, the scaling factor is the number of accessible local configurations, $\Sigma(\phi, U) = e^{S_2(\phi,U)}$; Σ and S_2 are both functions of packing fraction, ϕ, and the interparticle potential $U \equiv U(r, T)$. The finding $c < 1$ suggests that $\Sigma(\phi, U)/\Sigma(0, U)$ sets an upper limit for the long-time diffusion coefficients D^* in dense attractive colloidal fluids. In total, our work suggests that the excess entropy scaling law is valid for confined 2D colloidal fluids with short-range attraction strengths ($-U_{min}$) in the range of 0–4 $k_B T$. This finding enables quantitative estimation of long-time diffusion dynamics using static structural information.

IV. SUMMARY

We report experiments that elucidate the effects of short-range attractive forces on liquid structure and diffusion dynamics in 2D colloidal fluids. At fixed packing fractions, we find that stronger attraction gives rise to enhanced short-range correlation between nearest neighbors and reduced longer-range correlations. The measurements also clearly show that particle density fluctuations become more spatially heterogeneous in space and in time (at intermediate time scales) in samples with stronger attraction. These effects are ultimately consequences of the formation of transient colloidal clusters whose sizes and lifetimes increase with packing fraction and interparticle attraction strength. We calculate the two-body excess entropy S_2 from $g(r)$ and find that S_2 decreases monotonically with increasing attraction strength. Thus, although the structure of the colloidal fluids becomes more heterogeneous with stronger short-range attraction, on average, these systems are more ordered than repulsive systems of the same concentration. These effects contrast substantially with those found for systems with long-range attractive forces.[36] Finally, we corroborated the connection between two-body excess entropy and long-time diffusion, which exhibited the scaling form $D/D_0 = e^{cS_2}$. The work provides structure-dynamics data about colloidal fluids in an important regime, and the results offer insights for understanding rheological properties of suspensions from a structural perspective.[25–28] Looking forward, the demonstrated utility of the excess entropy concept in fluidic systems with short-range attractions also offers a simplified approach, based on the structure, to understand the re-entrant glass transition induced by short-range attractions.[29,32,34]

ACKNOWLEDGMENTS

We thank Kevin Aptowicz, Remi Dreyfus, Chandan Mishra, and Peter Collings for helpful discussions. J.C.L., X.G.M., and A.G.Y. gratefully acknowledge financial support from the National Science Foundation through Grant No. DMR16-07378, the Penn MRSEC Grant No. DMR-1720530, including its Optical Microscopy Shared Experimental Facility, and NASA No. NNX08AO0G.

REFERENCES

[1] N. W. Ashcroft and N. D. Mermin, *Solid State Physics* (Rinehart and Winston, New York, 1976).

[2] J. P. Hansen and I. R. McDonald, *Theory of Simple Liquids* (Academic Press, London, 986).

[3] Y. Rosenfeld, "Relation between the transport coefficients and the internal entropy of simple systems," Phys. Rev. A **15**, 2545–2549 (1977).

[4] Y. Rosenfeld, "A quasi-universal scaling law for atomic transport in simple fluids," J. Phys.: Condens. Matter **11**(28), 5415 (1999).

[5] M. Dzugutov, "A universal scaling law for atomic diffusion in condensed matter," Nature **381**(6578), 37–139 (1996).

[6] M. Dzugutov, "Dynamical diagnostics of ergodicity breaking in supercooled liquids," J. Phys.: Condens. Matter **11**(10A), A253–A259 (1999).

[7] A. Baranyai and D. J. Evans, "Direct entropy calculation from computer simulation of liquids," Phys. Rev. A **40**, 3817–3822 (1989).

[8] J. J. Hoyt, M. Asta, and B. Sadigh, "Test of the universal scaling law for the diffusion coefficient in liquid metals," Phys. Rev. Lett. **85**, 594–597 (2000).

[9] W. Götze, *Complex Dynamics of Glass-Forming Liquids: A Mode-Coupling Theory* (Oxford University Press, New York, 2008).

[10] A. Samanta, Sk. M. Ali, and S. K. Ghosh, "Universal scaling laws of diffusion in a binary fluid mixture," Phys. Rev. Lett. **87**, 245901 (2001).

[11] Y. Rosenfeld, "Excess-entropy and freezing-temperature scalings for transport coefficients: Self-diffusion in Yukawa systems," Phys. Rev. E **62**, 7524–7527 (2000).

[12] J. Mittal, J. R. Errington, and T. M. Truskett, "Thermodynamics predicts how confinement modifies the dynamics of the equilibrium hard-sphere fluid," Phys. Rev. Lett. **96**, 77804 (2006).

[13] W. P. Krekelberg, M. J. Pond, G. Goel, V. K. Shen, J. R. Errington, and T. M. Truskett, "Generalized Rosenfeld scalings for tracer diffusivities in not-so-simple fluids: Mixtures and soft particles," Phys. Rev. E **80**, 061205 (2009).

[14] M. J. Pond, J. R. Errington, and T. M. Truskett, "Communication: Generalizing Rosenfeld's excess-entropy scaling to predict long-time diffusivity in dense fluids of Brownian particles: From hard to ultrasoft interactions," J. Chem. Phys. **134**(8), 081101 (2011).

[15] J. C. Dyre, "Perspective: Excess-entropy scaling," J. Chem. Phys. **149**(21), 210901 (2018).

[16] X. G. Ma, W. Chen, Z. R. Wang, Y. Peng, Y. L. Han, and P. Tong, "Test of the universal scaling law of diffusion in colloidal monolayers," Phys. Rev. Lett. **110**, 078302 (2013).

[17] C.-H. Wang, S.-H. Yu, and P. Chen, "Universal scaling laws of diffusion in two-dimensional granular liquids," Phys. Rev. E **91**, 060201 (2015).

[18] J. D. Weeks, D. Chandler, and H. C. Andersen, "Role of repulsive forces in determining the equilibrium structure of simple liquids," J. Chem. Phys. **54**(12), 5237–5247 (1971).

[19] D. Chandler, J. D. Weeks, and H. C. Andersen, "Van der waals picture of liquids, solids, and phase transformations," Science **220**(4599), 787–794 (1983).

[20] L. Berthier and G. Tarjus, "Nonperturbative effect of attractive forces in viscous liquids," Phys. Rev. Lett. **103**, 170601 (2009).

[21] U. R. Pedersen, T. B. Schrøder, and J. C. Dyre, "Repulsive reference potential reproducing the dynamics of a liquid with attractions," Phys. Rev. Lett. **105**, 157801 (2010).

[22] Z. E. Dell and K. S. Schweizer, "Microscopic theory for the role of attractive forces in the dynamics of supercooled liquids," Phys. Rev. Lett. **115**, 05702 (2015).

[23] H. N. W. Lekkerkerker and R. Tuinier, *Colloids and the Depletion Interaction* (Springer Netherlands, New York, 2011).

[24] L. L. Hench and J. K. West, "The sol-gel process," Chem. Rev. **90**, 33 (1990).

[25] J. C. Conrad and J. A. Lewis, "Structure of colloidal gels during microchannel flow," Langmuir **24**(15), 7628–7634 (2008).

[26] M. Laurati, G. Petekidis, N. Koumakis, F. Cardinaux, A. B. Schofield, J. M. Brader, M. Fuchs, and S. U. Egelhaaf, "Structure, dynamics, and rheology of colloid-polymer mixtures: From liquids to gels," J. Chem. Phys. **130**(13), 134907 (2009).

[27] M. Laurati, S. U. Egelhaaf, and G. Petekidis, "Nonlinear rheology of colloidal gels with intermediate volume fraction," J. Rheol. **55**(3), 673–706 (2011).

[28] R. Pandey and J. C. Conrad, "Effects of attraction strength on microchannel flow of colloid-polymer depletion mixtures," Soft Matter **8**, 10695–10703 (2012).

[29] K. N. Pham, A. M. Puertas, J. Bergenholtz, S. U. Egelhaaf, A. Moussaıd, P. N. Pusey, A. B. Schofield, M. E. Cates, M. Fuchs, and W. C. K. Poon, "Multiple glassy states in a simple model system," Science **296**(5565), 104–106 (2002).

[30] W. P. Krekelberg, J. Mittal, V. Ganesan, and T. M. Truskett, "How short-range attractions impact the structural order, self-diffusivity, and viscosity of a fluid," J. Chem. Phys. **127**(4), 044502 (2007).

[31] W. P. Krekelberg, J. Mittal, V. Ganesan, and T. M. Truskett, "Structural anomalies of fluids: Origins in second and higher coordination shells," Phys. Rev. E 77, 041201 (2008).
[32] E. Zaccarelli and W. C. K. Poon, "Colloidal glasses and gels: The interplay of bonding and caging," Proc. Natl. Acad. Sci. U. S. A. 106(36), 15203–15208 (2009).
[33] C. K. Mishra, A. Rangarajan, and R. Ganapathy, "Two-step glass transition induced by attractive interactions in quasi-two-dimensional suspensions of ellipsoidal particles," Phys. Rev. Lett. 110, 188301 (2013).
[34] Z. Brown, M. J. Iwanicki, M. D. Gratale, X. G. Ma, A. G. Yodh, and P. Habdas, "Correlated rearrangements of disordered colloidal suspensions in the vicinity of the reentrant glass transition," Europhys. Lett. 115(6), 68003 (2016).
[35] J. R. Savage, D. W. Blair, A. J. Levine, R. A. Guyer, and A. D. Dinsmore, "Imaging the sublimation dynamics of colloidal crystallites," Science 314(5800), 795–798 (2006).
[36] J. Gapinski, J. Szymanski, A. Wilk, J. Kohlbrecher, A. Patkowski, and R. Holyst, "Size and shape of micelles studied by means of SANS, PCS, and FCS," Langmuir 26(12), 9304–9314 (2010).
[37] M. D. Gratale, T. Still, C. Matyas, Z. S. Davidson, S. Lobel, P. J. Collings, and A. G. Yodh, "Tunable depletion potentials driven by shape variation of surfactant micelles," Phys. Rev. E 93, 050601 (2016).
[38] L.-J. Chen, S.-Y. Lin, C.-C. Huang, and E.-M. Chen, "Temperature dependence of critical micelle concentration of polyoxyethylenated non-ionic surfactants," Colloids Surf., A 135(1), 175–181 (1998).
[39] J. N. Israelachvili, *Intermolecular and Surface Forces* (Academic Press, London, 1985).
[40] M. Piech and J. Y. Walz, "Depletion interactions produced by nonadsorbing charged and uncharged spheroids," J. Colloid Interface Sci. 232(1), 86–101 (2000).
[41] Y. Mao, M. E. Cates, and H. N. W. Lekkerkerker, "Depletion stabilization by semidilute rods," Phys. Rev. Lett. 75, 4548–4551 (1995).
[42] M. Polin, D. G. Grier, and Y. L. Han, "Colloidal electrostatic interactions near a conducting surface," Phys. Rev. E 76, 041406 (2007).
[43] D. A. Saville, W. B. Russel, and W. R. Schowalter, *Colloidal Dispersions* (Oxford University Press, New York, 1989).
[44] B. Cui, H. Diamant, B. Lin, and S. A. Rice, "Anomalous hydrodynamic interaction in a quasi-two-dimensional suspension," Phys. Rev. Lett. 92, 258301 (2004).
[45] V. N. Michailidou, G. Petekidis, J. W. Swan, and J. F. Brady, "Dynamics of concentrated hard-sphere colloids near a wall," Phys. Rev. Lett. 102, 068302 (2009).
[46] A. L. Thorneywork, R. E. Rozas, R. P. A. Dullens, and J. Horbach, "Effect of hydrodynamic interactions on self-diffusion of quasi-two-dimensional colloidal hard spheres," Phys. Rev. Lett. 115, 268301 (2015).
[47] T. Fischer, D. Weitz, Y. Peng, W. Chen, and P. Tong, "Short-time self-diffusion of nearly hard spheres at an oil-water interface," J. Fluid Mech. 618, 243 (2009).
[48] J. Happel and H. Brenner, *Low Reynolds Number Hydrodynamics: With Special Applications to Particulate Media* (Martinus Nijhoff Publishers, The Hague, Boston, 1983).
[49] E. R. Weeks, J. C. Crocker, A. C. Levitt, A. Schofield, and D. A. Weitz, "Three-dimensional direct imaging of structural relaxation near the colloidal glass transition," Science 287(5453), 627–631 (2000).
[50] W. K. Kegel and A. van Blaaderen, "Direct observation of dynamical heterogeneities in colloidal hard-sphere suspensions," Science 287(5451), 290–293 (2000).
[51] K. Zahn, J. M. Méndez-Alcaraz, and G. Maret, "Hydrodynamic interactions may enhance the self-diffusion of colloidal particles," Phys. Rev. Lett. 79, 175–178 (1997).